quarter chord at the 30% span station has been captured by the computations. The large variations in the computational results at the 30% span station near the trailing edge are due to surface variations associated with the trailing-edge control surface. The control surface was not instrumented with pressure ports so there are no pressure measurements available for this region. The comparison with the outboard span stations is poor, especially at the 60% station. Improved grid resolution is needed for the outboard span stations to capture the vortical flow phenomena in that region.[16]

A refined grid was generated and steady calculations performed and presented in Ref. 17. These results provided only a marginal improvement in the analysis test correlation in the vortical flow regions especially at 60% span. Some unsteady calculations have also been performed for the RSM on the OTT. These results are presented in Refs. 17 and 18.

Summary

A large database of steady, unsteady, and flutter wind-tunnel data has been obtained for three configurations based on an HSCT design: the RSM on a balance, the RSM on a PAPA, and the RSM on the OTT. The database covers an extensive Mach-number range from subsonic to low supersonic with a special emphasis on transonic conditions. The RSM was highly instrumented and the acquired database represents one of the largest aerodynamic and aeroelastic databases available. Examples of steady and unsteady pressure data were shown. The flutter behavior of the RSM on the PAPA mount was examined. Preliminary CFD analyses were performed and compared with experimental data. All of the RSM wind-tunnel data are available for public distribution.

References

[1]Corliss, J. M., and Cole, S. R., "Heavy Gas Conversion of the NASA Langley Transonic Dynamics Tunnel," *Proceedings of the 20th Advanced Measurements and Ground Testing Technology Conference*, NASA, Langley Research Center, Hampton, VA, June 1998.

[2]Cole, S. R., and Rivera, J. A., Jr., "The New Heavy Gas Testing Capability in the NASA Langley Transonic Dynamics Tunnel," *Royal Aeronautical Society Wind Tunnels and Wind Tunnel Test Techniques Forum*, The Royal Aeronautical Society, No. 4, Cambridge, England, UK, April 1997.

[3]Ruiz-Calavera, L. P., Bennett, R., Fox, J., Huang, X., Kaynes, I., Galbraith, R., Henshaw, M., Naudin, P., Geurts, E., Löser, T., and Tamayama, M., "A New Compendium of Unsteady Aerodynamic Test Cases for CFD: Summary of AVT WG-003 Activities," *International Forum on Aeroelasticity and Structural Dynamics*, Confederation of European Aerospace Societies (CEAS) and the AIAA, NASA Langley Research Center, Hampton, VA, June 1999.

[4]Bennett, R. M., Eckstrom, C. V., Rivera, J. A., Jr., Dansberry, B. E., Farmer, M. G., and Durham, M. H., "The Benchmark Aeroelastic Models Program: Description and Highlights of Initial Results," NASA TM 104180, April 1991.

[5]Durham, M. H., Keller, D. F., Bennett, R. M., and Wieseman, C. D., "A Status Report on a Model for Benchmark Active Controls Testing," AIAA Paper 91-1011, April 1991.

[6]Rivera, J. A., Jr., Dansberry, B. E., Bennett, R. M., Durham, M. H., and Silva, W. A., "NACA0012 Benchmark Model Experimental Flutter Results with Unsteady Pressure Distributions," NASA TM 107581, April 1992.

[7]Rivera, J. A., Jr., Dansberry, B. E., Durham, M. H., Bennett, R. M., and Silva, W. A., "Pressure Measurements on a Rectangular Wing with a NACA0012 Airfoil During Conventional Flutter," NASA TM 104211, July 1992.

[8]Dansberry, B. E., Durham, M. H., Bennett, R. M., Turnock, D. L., Silva, W. A., and Rivera, J. A., Jr., "Physical Properties of the Benchmark Models Program Supercritical Wing," NASA TM 4457, Sept. 1993.

[9]Scott, R. C., Hoadley, S. T., Wieseman, C. D., and Durham, M. H., "The Benchmark Active Controls Technology Model Aerodynamic Data," *Journal of Guidance, Control, and Dynamics*, Vol. 23, No. 5, 2000, pp. 914–921; also AIAA Paper 97-0829, Jan. 1997.

[10]Schuster, D. M., Spain, C. V., Turnock, D. L., Raush, R. D., Hamounda, M.-N., Vogler, W. A., and Stockwell, A. E., "Development, Analysis, and Testing of the High Speed Research Flexible Semispan Model," NASA CR 1999-209556, Sept. 1999.

[11]Scott, R. C., Silva, W. A., Florance, J. R., and Keller, D. F., "Measurement of Unsteady Pressure Data on a Large HSCT Semispan Wing and Comparison with Analysis," AIAA Paper 2002-1648, April 2002.

[12]Piatak, D. J., and Cleckner, C. S., "A New Forced Oscillation Capability for the Transonic Dynamics Tunnel," AIAA Paper 2002-0171, Jan. 2002.

[13]Schuster, D. M., and Rausch, R. D., "Transonic Dynamics Tunnel Force and Pressure Data Acquired on the HSR Rigid Semispan Model," NASA CR 1999-209555, Sept. 1999.

[14]Silva, W. A., Keller, D. F., Florance, J. R., Cole, S. R., and Scott, R. C., "Experimental Steady and Unsteady Aerodynamic and Flutter Results for HSCT Semispan Models," AIAA Paper 2000-1697, April 2000.

[15]Kris, S. L., Biedron, R. T., and Rumsey, C. L., "CFL3D User's Manual Version 5.0," NASA-TM 1998-208444, June 1998.

[16]Bartels, R. E., and Gatski, T. B., "Prediction of Transonic Vortex Flows Using Linear and Nonlinear Turbulent Eddy Viscosity Models," NASA-TM 2000-210282, May 2000.

[17]Scott, R. C., and Silva, W. A., "Pitch Oscillation Data and Analysis for a Large HSCT Semispan Wing," *AIAA/CEAS International Forum on Aeroelasticity and Structral Dynamics*, IFASD-US-38, Confederation of European Aerospace Societies (CEAS) and the AIAA, NASA Langley Research Center, Hampton, VA, Amsterdam, June 2003.

[18]Hong, M. S., Kuruvila, G., Bhatia, K. G., SenGupta, G., and Kim, T., "Evaluation of CFL3D for Unsteady Pressure and Flutter Predictions," AIAA Paper 2003-1932, April 2003.

Effects of Reynolds Number on Characteristics of Fixed and Rotary Wings

S. Sunada*
Osaka Prefecture University, Osaka 599-8531, Japan
and
K. Kawachi†
University of Tokyo, Tokyo 113-8656, Japan

Nomenclature

AR	=	aspect ratio
ARe	=	effective aspect ratio
b	=	number of wings
C_D	=	coefficient of drag of a wing, as indicated by Eq. (7)
C_{Dp}	=	profile drag, as indicated by Eq. (4)
C_d	=	coefficient of drag of an airfoil, $C_d(C_\ell = 0) + \delta_1(\alpha - \alpha_0) + \delta_2(\alpha - \alpha_0)^2$
C_L, C_ℓ	=	coefficients of lift of a wing and an airfoil, respectively
$C_{L\alpha}, C_{\ell\alpha}$	=	lift slope of a wing and an airfoil, respectively
C_T, C_Q	=	thrust and torque coefficients, respectively
c	=	chord length
R	=	diameter of a rotary wing
$\bar{R}$	=	ratio between profile drag proportional to $(\alpha - \alpha_0)^2$ and induced drag and induced drag, as indicated by Eq. (12)
Re	=	Reynolds number
r	=	spanwise position of a rotary wing
U	=	forward speed
W/S	=	wing loading
w	=	sinking speed
α	=	geometrical angle of attack

Received 27 May 2003; revision received 12 June 2003; accepted for publication 30 July 2003.

*Associate Professor, Department of Aerospace Engineering, Graduate School of Engineering; sunada@aero.osakafu-u.ac.jp.

†Professor, Department of Aeronautics and Astronautics. Associate Fellow AIAA.

α_i = induced angle of attack, $[C_L(\alpha)/\pi AR](1+\tau)$
α_0 = geometrical angle of attack of zero lift
γ = flight-path angle
Δ_k = coefficients of $(\alpha-\alpha_0)^k$ of C_D, $(k=1, 2)$
δ_k = coefficients of $(\alpha-\alpha_0)^k$ of C_d, $(k=1, 2)$
θ = collective pitch
θ_t = collective pitch at the wing tip
ρ = air density
σ = factor correcting the induced drag to allow for the change from elliptical span loading resulting from the use of a wing of rectangular planform
σ_s = solidity, $bc/\pi R$
τ = factor correcting the induced angle of attack to allow for the change from elliptical span loading resulting from the use of a wing of rectangular planform

Subscript

min = minimum value

Introduction

SUNADA et al. measured the characteristics of wings at an ultralow Reynolds number ($Re=4\times10^3$) (Refs. 1 and 2) and discussed the effect of three-dimensionality on the characteristics. Here, we improved the calculation model more exactly and represent the equations for the effect of three-dimensionality on the characteristics. Finally, we apply these corrected equations to a fixed wing in gliding flight and to a rotary wing in hovering flight.

Analysis

Sunada et al. expressed the drag coefficient C_D of a wing with an airfoil shape that is constant along the wing span, as follows:

$$C_D(\alpha)=C_d(\alpha)+\left[C_L^2(\alpha)\big/\pi AR\right](1+\sigma) \tag{1}$$

$$C_D(\alpha)=C_d(\alpha)+\left[C_L^2(\alpha)/\pi ARe\right] \tag{2}$$

Equations (1) and (2) are shown as Eq. (7) in Ref. 1 and Eq. (4) in Ref. 2, respectively. The first terms in the right-hand side in Eqs. (1) and (2) are profile drag, which can be estimated from the characteristics of an airfoil. The second terms are induced drag. Considering blade-element analysis, in the first terms in Eqs. (1) and (2), the effective angle of attack $(\alpha-\alpha_i)$, not the geometrical angle of attack α, should be used, when evaluating the value of C_d more precisely. Moreover, ARe in Eq. (2) is different from that widely used.[3] The equation for C_D widely used is

$$C_D=C_{\mathrm{Dp}}+\left(C_L^2\big/\pi AR\right)(1+\sigma)=C_{D\min}+C_L^2\big/\pi ARe \tag{3}$$

where

$$C_{\mathrm{Dp}}=C_{D\min}+kC_L^2 \tag{4}$$

and

$$ARe=\frac{AR}{1+\sigma+\pi kAR} \tag{5}$$

The AR_e in Eq. (5) includes the term of kC_L^2 in Eq. (4); on the other hand, that in Eq. (1) does not. Then, the definition of AR_e in Eq. (2) is different from that widely used.

According to these reasons, the following equation, instead of Eqs. (1) and (2), will be used for discussing the effect of three-dimensionality on the wing characteristics:

$$\begin{aligned}C_D(\alpha)&=C_d(\alpha-\alpha_i)+\left[C_L^2(\alpha)\big/\pi AR\right](1+\sigma)\\&=\left[C_d(C_\ell=0)+\delta_1(\alpha-\alpha_0-\alpha_i)+\delta_2(\alpha-\alpha_0-\alpha_i)^2\right]\\&\quad+\left[C_L^2(\alpha)\big/\pi AR\right](1+\sigma)\end{aligned} \tag{6}$$

The C_D can also be expressed as follows [see Eq. (2) in Ref. 1]:

$$C_D(\alpha)=C_D(C_L=0)+\Delta_1(\alpha-\alpha_0)+\Delta_2(\alpha-\alpha_0)^2 \tag{7}$$

Equating Eqs. (6) and (7), the following equations are obtained:

$$C_d(C_\ell=0)=C_D(C_L=0) \tag{8}$$

$$\delta_1=\frac{\Delta_1}{1-(1+\tau)(C_{L\alpha}/\pi AR)} \tag{9}$$

$$\delta_2=\frac{\Delta_2-(1+\sigma)\left(C_{L\alpha}^2\big/\pi AR\right)}{[1-(1+\tau)(C_{L\alpha}/\pi AR)]^2} \tag{10}$$

Equations (8–10) are modified from Eqs. (8–10) in Ref. 1, respectively.

Equation (10) shows that in Eq. (7) the term $\Delta_2(\alpha-\alpha_0)^2$, which is proportional to $(\alpha-\alpha_0)^2$, is

$$\begin{aligned}\Delta_2(\alpha-\alpha_0)^2&=\delta_2\left[1-(1+\tau)\frac{C_{L\alpha}}{\pi AR}\right]^2(\alpha-\alpha_0)^2\\&\quad+(1+\sigma)\frac{C_{L\alpha}^2}{\pi AR}(\alpha-\alpha_0)^2\end{aligned} \tag{11}$$

The term $\delta_2[1-(1+\tau)C_{L\alpha}/\pi AR]^2(\alpha-\alpha_0)^2$ is caused by profile drag, and the term $(1+\sigma)(C_{L\alpha}^2/\pi AR)(\alpha-\alpha_0)^2$ is induced drag. The ratio $\bar{R}$ between these two terms is

$$\begin{aligned}\bar{R}&=\delta_2\left[1-(1+\tau)\frac{C_{L\alpha}}{\pi AR}\right]^2\Bigg/(1+\sigma)\frac{C_{L\alpha}^2}{\pi AR}\\&=\left[\frac{\delta_2}{\pi AR(1+\sigma)}\right]\left(1+\tau-\frac{\pi AR}{C_{L\alpha}}\right)^2\end{aligned} \tag{12}$$

Table 1 shows the values of $C_D(C_L=0)=C_d(C_\ell=0)$, $C_{L\alpha}$, $C_{\ell\alpha}$, Δ_1, Δ_2, δ_1, δ_2, and $\bar{R}$ for wings of various airfoil shapes at various Reynolds numbers. The wing characteristics in this table are referred from Refs. 1, 6, and 7. The relation between $C_{L\alpha}$ and $C_{\ell\alpha}$ is

$$C_{\ell\alpha}=\frac{C_{L\alpha}}{1-(1+\tau)(C_{L\alpha}/\pi AR)} \tag{13}$$

Table 1 Characteristics for wings with various airfoil shapes at various Reynolds numbers

Airfoil shape	$C_D(C_L=0)$	$C_{L\alpha}$ / $C_{\ell\alpha}$	Δ_1 / δ_1	Δ_2 / δ_2	$\bar{R}$
Rectangle with 5% thickness ratio					
($Re=4\times10^3$) (Ref. 1)	6.4×10^{-2}	5.4	2×10^{-2}	5.0	2.6
		7.5	2.8×10^{-2}	7.0	
NACA0006					
($Re=4\times10^3$) (Ref. 1)	4.4×10^{-2}	4.3	-1.5×10^{-2}	2.8	2.2
		5.5	-1.9×10^{-2}	3.2	
($Re=6\times10^6$) (Ref. 6)	5.0×10^{-3}	4.5	-2.2×10^{-9}	1.1	0.11
		5.9	-2.9×10^{-9}	0.18	
NACA0009					
($Re=4\times10^4$) (Ref. 7)	1.6×10^{-2}	4.3	3.6×10^{-9}	1.7	0.95
		5.5	4.6×10^{-9}	1.4	
($Re=3\times10^5$) (Ref. 7)	6.8×10^{-3}	4.3	-2.3×10^{-8}	0.97	0.13
		5.5	-3×10^{-8}	0.18	
($Re=6\times10^6$) (Ref. 6)	5.5×10^{-3}	4.6	-1.0×10^{-9}	1.1	0.09
		6.1	-1.3×10^{-9}	0.16	

In the calculation of $\bar{R}$, the wing with a rectangular planform of $AR = 7.25$ and without twist are used . The values of τ and σ are 0.19 and 0.06, respectively.[4]

The $C_{\ell\alpha}$ of the rectangular airfoil with 5% thickness ratio is 7.5, which is larger than that expected by potential flow theory 2π. One possible reason for this discrepancy is that at an ultralow Reynolds number there is inaccuracy in Eq. (13), which is based on potential flow.

Based on the values of $\bar{R}$ in Table 1, the drag coefficient of a wing can be approximated as follows:

$$C_D(\alpha) \approx \begin{cases} C_d(C_\ell = 0) + (1+\sigma)C_L(\alpha)^2/\pi AR & Re > 10^5 \\ C_d(C_\ell = 0) \\ \quad + \delta_1\left[\alpha - \alpha_0 - (1+\tau)\dfrac{C_L(\alpha)}{\pi AR}\right] \\ \quad + \delta_2\left[\alpha - \alpha_0 - (1+\tau)\dfrac{C_L(\alpha)}{\pi AR}\right]^2 & \text{for} \quad 10^3 < Re < 10^5 \\ \quad + (1+\sigma)C_L(\alpha)^2/\pi AR \end{cases} \tag{14}$$

Equation (14) is an improvement of Eq. (5) in Ref. 2. Note that these approximations are not valid for airfoils with drag buckets such as laminar-flow airfoils.

Fixed Wing in Gliding Flight

Equation (14) reveals two conditions for optimal gliding. (Note that parasite drag on the body is ignored in this discussion and that only the wing is considered.) The first condition is for the minimum gliding flight-path angle $\gamma_{\min}$ (maximum flight range from a given height) and is given by $(\partial/\partial C_L)(C_D/C_L) = 0$. The other condition is for the minimum sinking speed $w_{\min}$ (maximum flight duration from a given height) and is given by $(\partial/\partial C_L)(C_D/C_L^{1.5}) = 0$.

1) For minimum gliding flight-path angle $\gamma_{\min}$, the optimal C_L and C_D are, respectively, given by

$$C_L = C_{L\alpha}\sqrt{\frac{[C_d(C_\ell = 0)/\delta_2]}{\left\{\left[1 - (1+\tau)\dfrac{C_{L\alpha}}{\pi AR}\right]^2 + (1+\sigma)\dfrac{C_{L\alpha}^2}{\pi AR\delta_2}\right\}}} \tag{15}$$

$$C_D = 2C_d(C_\ell = 0) + \delta_1[1 - (1+\tau)(C_{L\alpha}/\pi AR)] \times \sqrt{\frac{[C_d(C_\ell = 0)/\delta_2]}{\left\{\left[1 - (1+\tau)\dfrac{C_{L\alpha}}{\pi AR}\right]^2 + (1+\sigma)\dfrac{C_{L\alpha}^2}{\pi AR\delta_2}\right\}}} \tag{16}$$

2) For minimum sinking speed $w_{\min}$ the optimal C_L and C_D are, respectively, given by

$$C_L = 0.5C_{L\alpha}\left[1 - (1+\tau)\frac{C_{L\alpha}}{\pi AR}\right]\left(1 + \sqrt{1 + 12\left[\frac{C_d(C_\ell = 0)}{\delta_1}\right]\left\{\frac{\delta_2}{\delta_1} + \frac{(1+\sigma)\left(C_{L\alpha}^2/\pi AR\delta_1\right)}{[1 - (1+\tau)(C_{L\alpha}/\pi AR)]^2}\right\}}\right) \times \left\{(1+\sigma)\frac{C_{L\alpha}^2}{\pi AR\delta_1} + \frac{\delta_2}{\delta_1}\left[1 - (1+\tau)\frac{C_{L\alpha}}{\pi AR}\right]^2\right\}^{-1} \tag{17}$$

$$C_D = 4C_d(C_\ell = 0) + \delta_1\left[1 - (1+\tau)\frac{C_{L\alpha}}{\pi AR}\right]^2\left[1 + \sqrt{1 + 12\left[\frac{C_d(C_\ell = 0)}{\delta_1}\right]\left\{\frac{\delta_2}{\delta_1} + \frac{(1+\sigma)\left(C_{L\alpha}^2/\pi AR\delta_1\right)}{[1 - (1+\tau)(C_{L\alpha}/\pi AR)]^2}\right\}}\right] \times \left\{(1+\sigma)\frac{C_{L\alpha}^2}{\pi AR\delta_1} + \frac{\delta_2}{\delta_1}\left[1 - (1+\tau)\frac{C_{L\alpha}}{\pi AR}\right]^2\right\}^{-1} \tag{18}$$

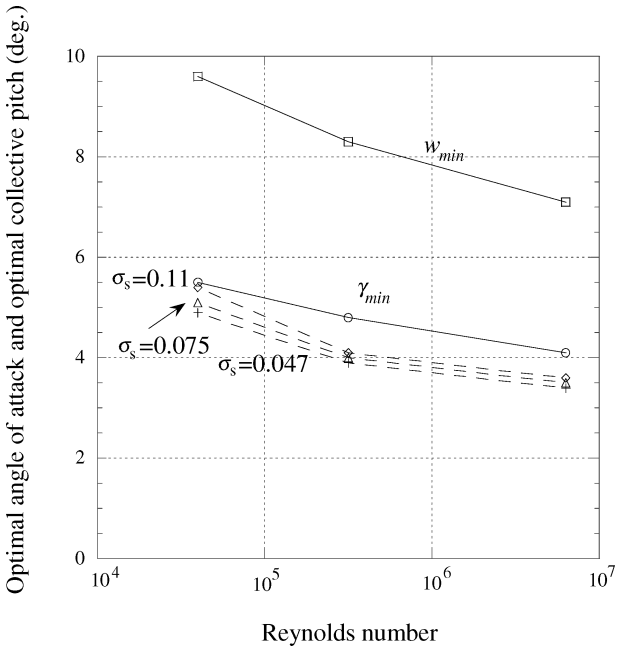

Fig. 1 Optimal angle of attack of a fixed wing in a gliding flight and optimal collective pitch at the tip of rotary wings in a hovering flight.

For each condition forward speed $U = \sqrt{\{2[(W/S)/\rho C_L]\}}$, gliding flight-path angle $\gamma \approx C_D/C_L$, and sinking speed $w \approx U(C_D/C_L)$ are obtained by using the preceding C_L and C_D. The δ_1 and δ_2 can be both set to 0 in Eqs. (15–18) at a high Reynolds number $Re > 10^5$. Equations (15–18) show improvements of Table 2 in Ref. 2.

Figure 1 shows the calculated $\gamma_{\min}$ and $w_{\min}$ as a function of Reynolds number for the wing with the airfoil shape of NACA0009, the rectangular planform of $AR = 7.25$, and no twist. The angles of attack for both $\gamma_{\min}$ and $w_{\min}$ increase with decreasing Reynolds number.

Rotary Wings in Hovering Flight

Here, thrust and torque acting on rotary wings in hovering flight are estimated by blade-element theory and simple momentum theory.[5] Note that in this estimation induced velocity is a constant at any spanwise position of the wings. The collective pitch θ at spanwise position r is assumed to be $\theta = \theta_t r/R$. The C_T/σ_s and C_Q/σ_s are expressed as

$$\frac{C_T}{\sigma_s} = \frac{C_{\ell\alpha}^2\sigma_s}{64}\left(1 + 16\frac{\theta_t}{C_{\ell\alpha}\sigma_s} - \sqrt{1 + 32\frac{\theta_t}{C_{\ell\alpha}\sigma_s}}\right) \tag{19}$$

$$\frac{C_Q}{\sigma_s} = \frac{C_T}{\sigma_s}\sqrt{\frac{C_T}{2}} + \left[\frac{C_{d0}}{8} + \frac{2}{3}\frac{C_T}{\sigma_s}\frac{\delta_1}{C_{\ell\alpha}} + 4\left(\frac{C_T}{\sigma_s}\right)^2\frac{\delta_2}{C_{\ell\alpha}^2}\right] \tag{20}$$

Figure 1 shows the estimated θ_t for maximum C_T/C_Q for a rotary wing whose airfoil shape is NACA0009 (Table 1) at $\sigma_s = 0.11$, 0.075, and 0.047. The θ_t for maximum C_T/C_Q decreases with increasing Reynolds number. Moreover, the collective pitch for maximum C_T/C_Q slightly increases with increasing solidity σ_s.

Conclusion

Effects of characteristics of an airfoil on those of a fixed wing under various Reynolds numbers were reanalyzed by the improved calculation model. At a low Reynolds number ($10^3 < Re < 10^5$) a component in profile drag proportional to the second-power of angle of attack cannot be ignored in comparison with induced drag. Then, a difference between AR and AR_e increases. Note that this difference between AR and AR_e for a wing with elliptical planform is not small at a low Reynolds number, and this result is not valid for airfoils with drag buckets such as laminar-flow airfoils. In addition, the calculation results indicate that a geometrical angle of attack for an optimal flight is larger with the decrease of Reynolds number.

In addition, effects of characteristics of an airfoil on those of rotary wings under various Reynolds numbers were analyzed. Similarly with a geometrical angle of attack of a fixed wing for an optimal flight, collective pitch of a rotary wing for an optimal hovering flight is increased with the decrease of Reynolds number.

References

[1]Sunada, S., Yasuda, T., Yasuda, K., and Kawachi, K., Comparison of Wing Characteristics at an Ultralow Reynolds Number, *Journal of Aircraft*, Vol. 39, No. 2, 2002, pp. 331–338.

[2]Sunada, S., Sakaguchi, A., and Kawachi, K., Airfoil Section Characteristics at a Low Reynolds Number, *Journal of Fluids Engineering*, Vol. 119, March 1997, pp. 129–135.

[3]McCormick, B. W., *Aerodynamics, Aeronautics and Flight Mechanics*, Wiley, New York, 1995, Chap. 4.

[4]Glauert, H. M. A., *The Elements of Aerofoil and Airscrew Theory*, Cambridge Univ. Press, Cambridge, England, U.K., 1926, Chap. 11.

[5]Prouty, R. W., *Helicopter Performance, Stability, and Control*, Krieger, Malabar, FL, 1990, Chap. 1.

[6]Abbott, I. H., and Doenhoff, A. E. V., "*Theory of Wing Sections*, Dover, New York, 1958, pp. 454, 455.

[7]Jacobs, E. N., and Sherman, A., Airfoil Section Characteristics as Affected by Variations of the Reynolds Number, NACA.TR-586, 1937.